AIAA JOURNAL
Vol. 55, No. 9, September 2017

Technical Notes

Experimental and Numerical Study on Hypersonic Flow over Double-Wedge Configuration

B. Q. Meng,* G. L. Han,† C. K. Yuan,‡ C. Wang,§ and Z. L. Jiang¶
State Key Laboratory of High Temperature Gas Dynamics, Chinese Academy of Sciences, 100190 Beijing, People's Republic of China

DOI: 10.2514/1.J055546

Nomenclature

H_a	=	second wedge height
H_f	=	first wedge height
H_t	=	total wedge height
H_0	=	total freestream enthalpy
i	=	along wall tangent direction
j	=	along wall normal direction
L	=	characteristic length (equal to H_t)
L_a	=	second wedge length
L_f	=	first wedge length
L_t	=	total wedge length
L_w	=	model width
M_a	=	Mach number
p	=	static pressure
p_0	=	total freestream pressure
Re	=	Reynolds number
T_0	=	total freestream temperature
α	=	first wedge angle
Δs	=	first cell height
δ	=	horizontal inclination of shock
θ	=	second wedge angle
ρ	=	density
∞	=	freestream

I. Introduction

THE engine inlet of an airbreathing hypersonic propulsion system consists of a series of exterior compression slopes that are responsible for obtaining upstream air and reducing the air flow Mach number. For the X-51 scramjet engine [1], the engine inlet can be simplified into a double-wedge configuration in a two-dimensional manner; shock/shock and shock wave/boundary layer interactions are typical characteristics.

Edney [2] classified six types of shock interactions in an experimental study that demonstrated the basic rules for shock/shock interaction classifications. Sullivan [3] put forward a series of equations to reveal the relationships of flow parameters between different regions for inviscid flow over a slender double wedge. Olejniczak et al. [4] used numerical simulation to study the shock interaction on a double wedge, and a new form of interaction was discovered. They used the computational fluid dynamics (CFD) method to study inviscid shock interactions on a double wedge, and different types of interactions have been identified [5]. The types and transitions of shock/shock interaction were observed, and only inviscid flowfields were considered in these studies.

Researchers have explored shock wave/boundary layer interaction via both numerical and experimental methods. Bertin and Hinkle [6] studied viscous/inviscid interaction characteristics with schlieren photographs, filming, and surface pressure measurements. Olejniczak et al. [7] conducted a series of experiments to test the flow over double-wedge geometries with nonequilibrium chemistry models; Reinartz et al. [8] explored the effects of shock wave/boundary layer interactions on wall temperatures and entropy layers.

Sinha et al. [9] studied the effect of turbulence on double-cone shock interactions. Computation of the type V interaction with a high Reynolds number showed that the turbulence solution was much closer to the experimental results than the laminar flow in terms of the separation zone size and peak pressure. Visualizations for various combinations of a first angle at 25 deg and a second angle at 40, 50, and 68 deg, respectively, were tested by Hashimoto et al. [10]; the results created an interferogram for the flowfield at various wedge angles by comparison.

Swantek and Austin [11] conducted experiments to investigate shock wave/boundary-layer interactions and the resulting heat transfer of a double wedge with air and nitrogen hypersonic flows, as well as an analysis of the detailed flowfield features in high-quality schlieren images; the shock/shock interaction they observed belonged to type IV. Furthermore, Badr and Knight [12] compared their CFD simulation results with the experimental results that were conducted by Swantek and Austin [11], and the heat transfer distributions were in accordance with the experimental results.

Komives et al. [13] conducted a numerical study on unsteady heat transference with double-wedge geometry; their results showed reasonable agreement with the experimental heating results, apart from some differences between the predicted and experimental flow structures. Later, researchers conducted a study on double-wedge geometry for which the first wedge angle was 9 deg and the second wedge angle was 20.5 deg [14]. Numerical results and experimental results were compared at different surface temperatures and nose radii. The influences of turbulence models, chemistry models in high-enthalpy flow, unsteadiness, entropy layers, nose radii, and other factors were investigated with particular focus on heat transfer and pressure. However, few researchers to date have conducted quantitative comparisons between experiments and the numerical results for wave structures.

This Note aims to provide a comprehensive comparison between experimental and numerical wave structures. Experiments were conducted in a detonation-driven long-test-duration shock tunnel [15] (JF12 hypersonic shock tunnel). Numerical results were derived from the Euler equation to study the shock-dominated flowfield; the effects of separation in the boundary layer were simulated via Navier–Stokes equations. A comparison among angles of the shock

Received 27 July 2016; revision received 28 February 2017; accepted for publication 14 April 2017; published online 27 June 2017.

*Ph.D. Student, Institute of Mechanics; also University of Chinese Academy of Sciences, 100049 Beijing, People's Republic of China. Student Member AIAA.

†Assistant Professor, Institute of Mechanics; also University of Chinese Academy of Sciences, 100049 Beijing, People's Republic of China; hanguilai@imech.ac.cn (Corresponding Author).

‡Engineer, Institute of Mechanics; also University of Chinese Academy of Sciences, 100049 Beijing, People's Republic of China.

§Associate Professor, Institute of Mechanics; also University of Chinese Academy of Sciences, 100049 Beijing, People's Republic of China.

¶Professor, Institute of Mechanics; also University of Chinese Academy of Sciences, 100049 Beijing, People's Republic of China. Associate Fellow AIAA.

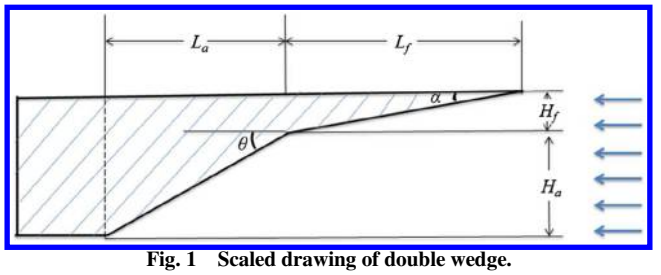

Fig. 1 Scaled drawing of double wedge.

and slip lines was obtained by various methods, as will be discussed in the following.

II. Experimental Program

A. Visualization System

The visualization system used in this study contains a xenon lamp as an optical source, reflecting mirrors M1–M4, and a high-speed camera (Photron SA4) that can capture 3600 frames per second, with resolution of 1024×1024.

B. Experimental Model and Freestream Conditions

The configuration of the double wedge applied in the tests is illustrated in Fig. 1. The inclination and lengths of wedges are listed in Table 1. The angles of approach in all cases are almost 0 deg. Table 2 lists the Mach number, total pressure, and total temperature of the nozzles. The standard deviation of the Mach numbers of three shots is lower than 0.03, and accurate repetition was performed. The total enthalpy H_0 was about 2.23 MJ/kg. Schlieren images were captured in every test to ensure accurate quantitative comparisons of the wave structures.

C. Experimental Results

The schlieren results of the experiments are presented in Fig. 2. The shock/shock interaction in the double wedge is a type VI interaction according to Edney's classification [2]. Attached to the leading-edge oblique, shock AD formed when upstream flows occurred over ramp AB while the boundary layer on the first wedge developed. The flow separated at point P, where the separation shock wave formed. The flow reattached near point Q, which caused a strong interaction between the shock wave and boundary layer. A reattachment shock, QD, also formed and intersected with shock AD at point D. This interaction formed slip line DE and shock DF. Figure 2 shows shocks AD, QD, and DF. The separation shock is very weak compared to all three shocks.

Table 1 Double wedge configuration

Definition	Symbol	Value
First wedge length	L_f	110.0 mm
Second wedge length	L_a	83.8 mm
Total wedge length	L_t	193.8 mm
First wedge height	H_f	19.4 mm
Second wedge height	H_a	48.4 mm
Total wedge height	H_t	67.8 mm
Model width	L_w	170 mm
First wedge angle	α	10.0 deg
Second wedge angle	θ	30.0 deg

Table 2 Test conditions in the JF12 hypersonic tunnel

Parameter	Value
p_0, MPa	2.26
T_0, K	2217
Ma_∞	7.01
Re_∞	8.5×10^5/m

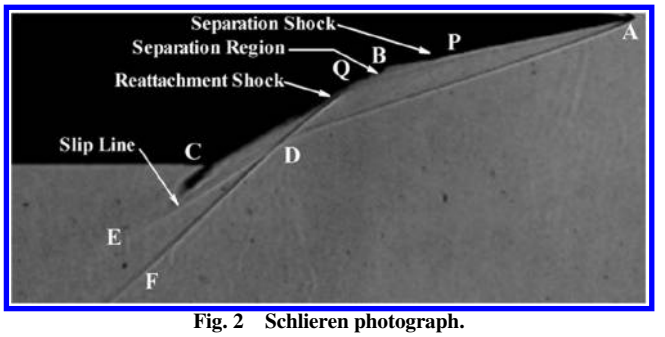

Fig. 2 Schlieren photograph.

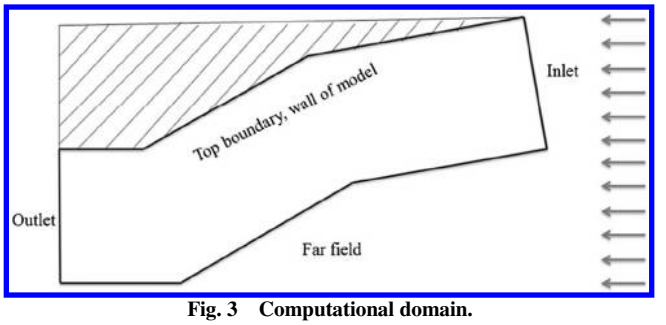

Fig. 3 Computational domain.

III. Numerical Method and Results

A. Computational Domain and Grid Generation

The computational domain contains the four boundaries shown in Fig. 3. Structured mesh orthogonality was ensured by using Akcelik et al.'s method [16]. A total of four separate grids was used for grid refinement to check grid convergence. Each grid was obtained from the previous grid by doubling the grid number in both directions. The grid spacing near the wall in the normal direction was intensive, and the ratio of stretching from the normal direction into the wall was roughly 1.01. The first cell Δs, with a resolution of 8161×1601, was 0.01 mm in height; the aspect ratio in the first cell was about three in all cases.

B. Governing Equations and Algorithm

Flow over the double wedge was simulated by solving the two-dimensional planar, compressible Navier–Stokes equation with a transformation into computational space [17]. The convective term was discretized by non-oscillatory, containing no free parameters and dissipative (NND) scheme [18] and viscous term were discretized by applying the second-order central difference method. The Runge–Kutta method [17] was applied for first-order and explicit time discretization; and the Courant–Friedrichs–Lewy number as 0.1. The local time step method [17] was used to speed up convergence, where the initial computational time steps were set to 50,000 in our case. We applied a global time step to maintain a steady solution. The criteria defined in Eq. (1) were applied to monitor the convergence to a steady state. When the magnitude of errors fell to less than 1% of the initial errors, the computation was halted. The numerical parameters of the upstream flow condition were consistent with the experimental parameters, and $\gamma = 1.4$:

$$\text{err} = \frac{\sum_{i=1}^{N_i} \sum_{j=1}^{N_j} (\rho_{(i,j)}^{n+1} - \rho_{(i,j)}^{n})^2}{N_i \cdot N_j} \tag{1}$$

C. Grid-Independence Verification

Our simulation results were sensitive to the number of resolutions. The Navier–Stokes equation, as mentioned previously, was used to check for grid convergence. Figure 4 is a plot of the wall pressure normalized by the freestream pressure for four different mesh results in the given time window. The 1021×201 and 2041×401 grids missed both the peak values of pressure, position, and separation

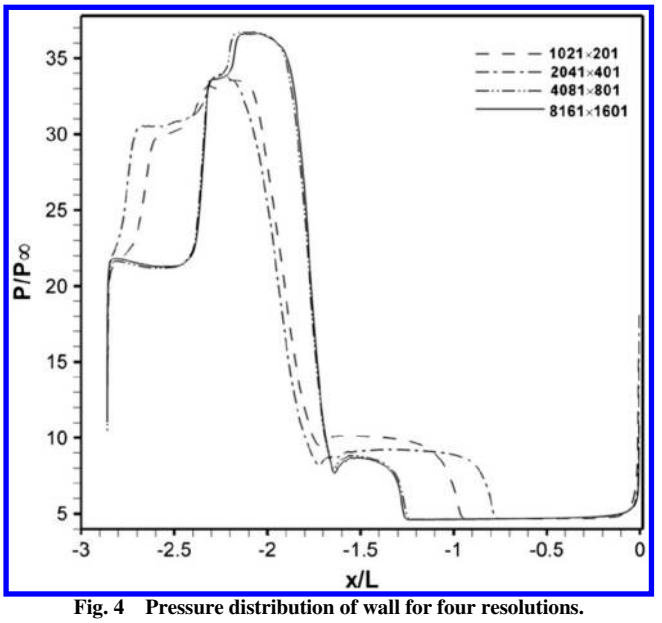

Fig. 4 Pressure distribution of wall for four resolutions.

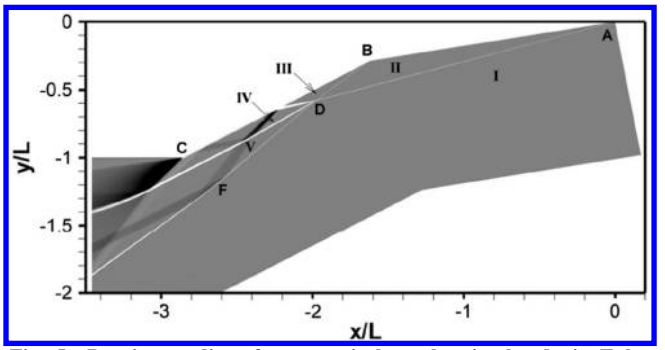

Fig. 5 Density gradient for numerical results simulated via Euler equation.

zone scale. The results of the 4081 × 801 resolution fit well with the results of the 8161 × 1601 resolution, suggesting that the refinement we conducted did not significantly affect the simulation. Thus, the 8161 × 1601 resolution was selected for all subsequent simulations.

D. Numerical Results Simulated with Euler Equation

Simulations were conducted via the Euler equation to study shock-dominated flowfields. A simple theoretical study based on oblique equation relationships was also performed. The parameters of the wave structures were compared across these two methods.

The wave structures of shocks AD and DF and of slip line DE were consistent with the results of the experiment, as shown in Fig. 5. Neglecting the viscidity factor caused the separation region to disappear entirely. The expansion wave emitted from the point interacted with the slip line and shock DF; then, it reflected off of the wall. Shock wave DF was weakened after point F. The Mach numbers in each side of the expansion fan were close, and the expansion wave was very weak. The flow parameters are listed in Table 3 for each region.

Table 3 Mach number Ma and angle values by inviscid simulation and theory

	Mach number Ma		Angle	
Region	Euler equation	Theory	Euler equation	Theory
I	7.0	7.0	— —	— —
II	5.3	5.3	$\delta_{AD} = 16.3$ deg	$\delta_{AD} = 16.4$ deg
III	3.1	3.1	$\delta_{BD} = 39.4$ deg	$\delta_{BD} = 39.3$ deg
IV	3.2	3.1	$\delta_{DE} = 31.2$ deg	$\delta_{DE} = 37.1$ deg
V	2.2	1.8	$\delta_{DF} = 42.7$ deg	$\delta_{DF} = 49.6$ deg

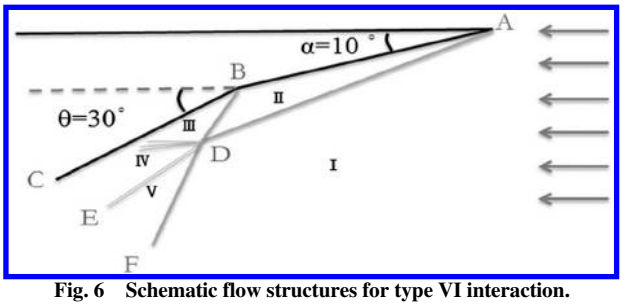

Fig. 6 Schematic flow structures for type VI interaction.

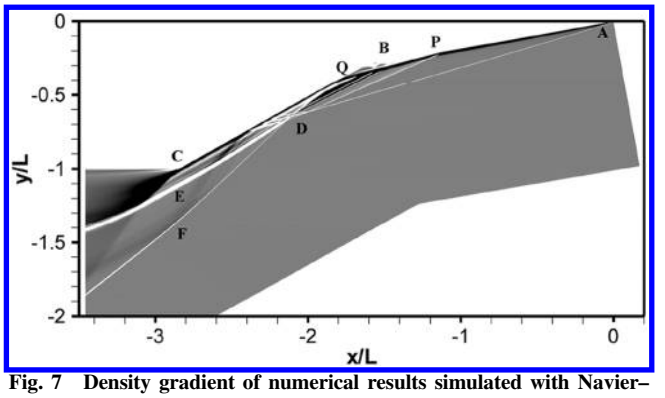

Fig. 7 Density gradient of numerical results simulated with Navier–Stokes equation.

A simple theoretical solution for inviscid flow based on oblique shock relations [19] was established. Based on the experimental results shown in Fig. 2d, schematic flow structures consisting of five regions are shown in Fig. 6.

1) From region I to region II, the parameters of region II and the AD angle can be solved directly per the classical oblique shock relationship according to Ma_I and the freestream parameters.

2) From region II to region III, the parameters of region III and the BD angle can also be solved by the oblique shock relationship.

3) From region III to region IV, the numerical and experimental results show that the expansion wave between region III and region IV is very weak, so region III and region IV parameters are considered to be consistent.

4) From region IV to region V, slip line ED exists between region IV and region V. The static pressure of the two sides of slip line ED are equal; that is, $p_{IV} = p_V$, so the P_V/P_I value can be calculated accordingly.

5) From region I to region V, the angle of shock DF (δ_{DF}) can be calculated based on the value of p_V/p_I and the Mach number of the freestream.

The comparisons of the values calculated by theoretical and inviscid simulations are given in Table 3. Values in region I, region II, and region III of the theoretical results agreed with the inviscid flow results, but there were some differences in the parameters in regions IV and V. The neglect of the expansion waves between region III and region IV caused these differences. The static pressure of region V, which was equal to the theoretical value of P_{IV}, exceeded the numerical results. The angle of shock DF was larger than the numerical results as well, suggesting that shock wave DF was stronger than the numerical results suggested.

E. Numerical Results Simulated with Navier–Stokes Equation

A numerical simulation by Navier–Stokes equation was conducted to further explore the flowfield. The wave structures shown in Fig. 7 are consistent with the experimental results, including edge shock AD, the separation shock wave, the reattachment shock wave, shock DF, and slip line DE. However, the positions of separation and reattachment were not in agreement with the experimental results. As shown in Fig. 2d, the flow separated at point P and AP/AB ≈ 0.78; the flow reattached at point Q and BQ/BC ≈ 0.21. As shown in Fig. 7, AP/AB ≈ 0.70 and BQ/BC ≈ 0.19. Turbulent flow and

Table 4 δ_{DE} and δ_{DF} values of four results

		Numerical simulation	
	Experiment	Navier–Stokes equation	Euler equation
δ_{DE}	33.1 deg	32.3 deg	31.2 deg
δ_{DF}	44.4 deg	44.2 deg	42.7 deg

three-dimensional effects were the main factors contributing to the inconsistency we observed [9,10] and merit further evaluation.

IV. Comparison

The results obtained by different methods are presented in Table 4. The values of angles DF and DE were selected as typical parameters for comparison. Navier–Stokes simulation results showed the best agreement with the experimental values, whereas the Euler equation results tended to underestimate the experimental values. Due to the neglect of the expansion wave, there were differences in the experimental values and results calculated by any of the theoretical methods.

V. Conclusions

In this study, experiments on a hypersonic flow over a double wedge were conducted in a JF12 hypersonic shock tunnel. Numerical simulations were also conducted by solving Euler and Navier–Stokes equations. Schlieren photographs of the experiments showed that the shock/shock interaction belonged to type VI. The basic wave structures of the Navier–Stokes and Euler numerical results were in accordance with the experimental results.

Quantitative comparisons for shock angles and slip lines were conducted for four sets of results to find that the Navier–Stokes angles showed the closest agreement with the experimental results. Conversely, the Euler equation simulations were slightly smaller than the experimental values. Further research is yet necessary to investigate the differences in separation and reattachment positions between the experimental and numerical results presented here.

Acknowledgments

This project was supported by the National Natural Science Foundation of China (grants 11472281 and 11532014) and the National Key Research and Development Program (no. 2016YFA0401201).

References

[1] Hank, J., Murphy, J., and Mutzman, R., "The X-51A Scramjet Engine Flight Demonstration Program," AIAA Paper 2008-2540, May 2008. doi:10.2514/6.2008-2540

[2] Edney, B., "Anomalous Heat Transfer and Pressure Distributions on Blunt Bodies at Hypersonic Speeds in the Presence of an Impinging Shock," Aeronautical Research Inst. of Sweden (FFA) Rept. 115, Stockholm, 1968.

[3] Sullivan, P. A., "Hypersonic Flow over Slender Double Wedges," *AIAA Journal*, Vol. 1, No. 8, 1963, p. 1927. doi:10.2514/3.1961

[4] Olejniczak, J., Wright, M. J., and Candler, G., "Numerical Study of Shock Interactions on Double-Wedge Geometries," AIAA Paper 1996-0041, Jan. 1996. doi:10.2514/6.1996-41

[5] Olejniczak, J., Wright, M., and Candler, G., "Numerical Study of Inviscid Shock Interactions on Double-Wedge Geometries," *Journal of Fluid Mechanics*, Vol. 352, Dec. 1997, pp. 1–25. doi:10.1017/S0022112097007131

[6] Bertin, J. J., and Hinkle, J. C., "Experimental Investigation of Supersonic Flow Past Double-Wedge Configurations," *AIAA Journal*, Vol. 13, No. 7, 1975, pp. 897–901. doi:10.2514/3.60466

[7] Olejniczak, J., Candler, G., and Wright, M. J., "High Enthalpy Double-Wedge Experiments," AIAA Paper 1996-2238, June 1996. doi:10.2514/6.1996-2238

[8] Reinartz, B., Ballmann, J., and Boyce, R., "Numerical Investigation of Wall Temperature and Entropy Layer Effects on Double Wedge Shock/Boundary Layer Interactions," AIAA Paper 2006-8137, 2006. doi:10.2514/6.2006-8137

[9] Sinha, K., Wright, M., and Candler, G., "The Effect of Turbulence on Double-Cone Shock Interaction," AIAA Paper 1999-0146, Jan. 1999. doi:10.2514/6.1966-756

[10] Hashimoto, T., Itoh, K., and Takayama, K., "Flow Feature Induced Separation over Double Wedges," AIAA Paper 2004-1135, Jan. 2004. doi:10.2514/6.2004-1135

[11] Swantek, A., and Austin, J., "Heat Transfer on a Double Wedge Geometry in Hypervelocity Air and Nitrogen Flows," AIAA Paper 2012-0284, Jan. 2012. doi:10.2514/6.2012-284

[12] Badr, M. A., and Knight, D. D., "Shock Wave Laminar Boundary Layer Interaction over a Double Wedge in a High Mach Number Flow," AIAA Paper 2014-1136, Jan. 2014. doi:10.2514/6.2014-1136

[13] Komives, J. R., Nompelis, R., and Candler, G. V., "Numerical Investigation of Unsteady Heat Transfer on a Double Wedge Geometry in Hypervelocity Flows," AIAA Paper 2014-2354, June 2014. doi:10.2514/6.2014-2354

[14] Reinartz, B., and Ballmann, J., *Shock Waves*, Springer, Berlin, 2009, pp. 1099–1104.

[15] Jiang, Z., and Yu, H. R., "Experiments and Development of Long-Test-Duration Hypervelocity Detonation-Driven Shock Tunnel (LHDst)," AIAA Paper 2014-1012, Jan. 2014.

[16] Akcelik, V., Jaramaz, B., and Ghattas, O., "Nearly Orthogonal Two-Dimensional Grid Generation with Aspect Ratio Control," *Journal of Computational Physics*, Vol. 171, No. 2, 2001, pp. 805–821. doi:10.1006/jcph.2001.6811

[17] Hoffmann, K. A., and Chiang, S. T., *Computational Fluid Dynamics*, Engineering Education System, Wichita, KS, 2000, pp. 69–85.

[18] Zhang, H. X., "NND Schemes and Numerical Simulation of Axial Symmetric Free Jet Flows," *Acta Mechanica Sinica*, Vol. 6, No. 3, 1990, pp. 193–203. doi:10.1007/BF02487640

[19] Anderson, I. D., *Modern Compressible Flow: With Historical Perspective*, International ed., Elizabeth A. Jones, New York, 2003, pp. 133–145.

J. M. Austin
Associate Editor